Photodecomposition and Photooxidation of Hydrogen Sulfite in Aqueous Solution

Michael Fischer and Peter Warneck*

Max-Planck-Institut für Chemie, 55020 Mainz, Germany

Received: November 1, 1995; In Final Form: February 14, 1996[⊗]

A zinc arc lamp and a mercury lamp, respectively, were used to study the photodecomposition of HSO_3^- and SO_3^{2-} in aqueous solutions saturated with either argon or nitrous oxide. The main products in both cases were sulfate and dithionate, which are attributed to arise from the self-reaction of SO_3^- radicals. Quantum yields for the formation of SO_3^- in argon-saturated solution based on hydrazoic acid and/or ferric oxalate actinometry were 0.19 ± 0.03 for HSO_3^- and 0.39 ± 0.03 for SO_3^{2-}, essentially independent of S(IV) concentration. In both systems, the rate of sulfate formation rose with time at the expense of that of dithionate. This is explained by reactions of hydrogen atoms and hydrated electrons with dithionate (rate coefficient $k_5 \approx 2 \times 10^5$ dm^3 mol^{-1} s^{-1}). N_2O as a scavenger for these radicals removed the effect and raised the quantum yields to 0.25 ± 0.03 and 0.75 ± 0.04, respectively. The product ratios under these conditions were $[S_2O_6^{2-}]/[SO_4^{2-}] = 0.43 \pm 0.04$ for HSO_3^- and 0.61 ± 0.03 for SO_3^{2-}. In oxygen-saturated solutions, the photolysis of HSO_3^- led to a short chain reaction with sulfate and peroxodisulfate as products. The latter product was assigned to arise from the recombination of SO_5^- radicals. Steady state analysis of the product evolution with time gave rate coefficients for two of the reactions involved: $k_{16}(SO_5^- + HSO_3^-) = (1.2 \pm 0.4) \times 10^4$ dm^3 mol^{-1} s^{-1} for the main propagation reaction and $k_{19a}(HO_2 + SO_5^-) = (1.8 \pm 1.0) \times 10^9$ dm^3 mol^{-1} s^{-1} for the principal termination reaction. These values agree well with recent data from radiolysis experiments.

Introduction

The autoxidation of sulfur(IV), that is, sulfite (SO_3^{2-}) and hydrogen sulfite (HSO_3^-) in aqueous solution, is now well known to occur by a chain reaction propagated by oxysulfur radicals.[1] The species involved are the sulfite radical, SO_3^-, the peroxomonosulfate radical, SO_5^-, as originally proposed by Bäckström,[2] and the sulfate radical, SO_4^-, as suggested by Hayon et al.[3] The reaction chain is initiated by the formation of SO_3^-, which can be generated from sulfur(IV) by way of photolysis,[3−6] radiolysis,[7−9] autocatalysis,[10] or reaction with certain transition metal ions.[1] In the presence of oxygen, SO_3^- is rapidly converted to SO_5^-, which acts as the main chain carrier. The oxidation of sulfur(IV) by transition metals may also proceed via a nonradical mechanism,[1] but at least for iron it has been demonstrated that a chain reaction propagated by oxysulfur radicals is dominant.[11] However, the interaction of radicals with the metal ions complicates the system.

It has been shown that photolysis of SO_3^{2-} with light from a mercury lamp (253.7 nm wavelength) provides a convenient way of generating SO_3^- radicals in alkaline solutions,[6] where oxidation is rapid. In acidic solutions, however, sulfur(IV) exists predominantly as HSO_3^- (p$K \approx 7.2$). Compared with SO_3^{2-}, the absorption spectrum of HSO_3^- has its onset at shorter wavelength (see Figure 1), so that it is less accessible. We have explored the photolysis of HSO_3^- using light from a zinc arc lamp and found that photodecomposition yields SO_3^- radicals in a similar manner as photolysis of SO_3^{2-}. The present paper reports results for (i) the photolyses of HSO_3^- and (for comparison) SO_3^{2-} in solutions saturated with either argon or N_2O and (ii) the photooxidation of HSO_3^- in the presence of oxygen. The chain oxidation of HSO_3^- is less rapid than that of SO_3^{2-}, which allows us to derive from the data some information about the magnitude of the rate coefficients for the chain-propagating step and the principal termination reaction.

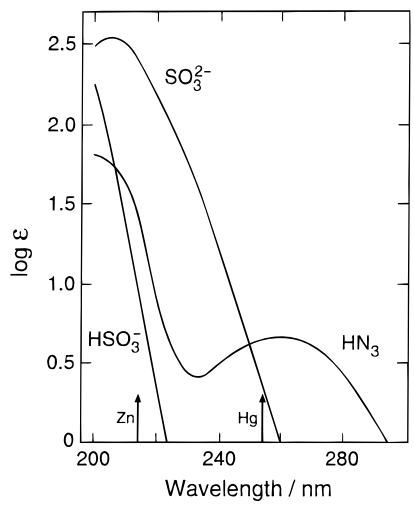

Figure 1. Decadic logarithm of absorption coefficients (unit: m^2 mol^{-1}) for HSO_3^-, SO_3^{2-}, and HN_3 in aqueous solution to indicate the positions of maxima and onsets in the spectra; data from Shapira and Treinin[13] and Deister et al.[14]

Experimental Section

Apparatus. Absorption coefficients were determined with a two-beam spectrophotometer (wavelength resolution 2 nm). The coaxial photolysis setup consisted of either a Penray low-pressure mercury lamp or a similarly rod-shaped zinc arc lamp, surrounded by a cylindrical quartz vessel (filling capacity ca. 50 cm^3). In the first case the photolysis cell was made of Haereus M235 quartz to eliminate radiation below 220 nm; in the second case Suprasil quartz was used. The radial distances between the vessels' concentric walls, which determined the absorption path lengths, were 1.15 and 1.3 cm, respectively. Whereas the mercury lamp radiated in all directions, the zinc lamp had the emission restricted to a 0.5 × 2 cm aperture. To achieve an even illumination of the solution, the quartz cell was placed on a turntable rotating at 10 rpm. Heat and ozone generated by the lamps were flushed out by means of com-

⊗ Abstract published in *Advance ACS Abstracts,* August 15, 1996.

S0022-3654(95)03236-9 CCC: $12.00

pressed air. After ignition, the lamps were given sufficient time to reach a stable output before they were placed inside the photolysis cells to initiate the photolysis.

Actinometry. Standard ferric oxalate actinometry[12] was used with the mercury lamp to determine the 253.7 nm photon flux entering the M235 quartz cell. At the lower wavelengths emitted by the zinc lamp the photolysis of hydrazoic acid, HN_3, in aqueous solution was used as actinometer.[13] The products of HN_3 photodecomposition are equivalent amounts of hydroxylamine and nitrogen, which are formed with quantum yields of unity. The products follow from the incipient formation of an excited HN_3* molecule and its reaction with water.[13] As shown in Figure 1, the absorption spectrum of HN_3 exhibits a moderately intense peak at 264 nm wavelength (decadic absorption coefficient $\epsilon_{max} = 4.63$ m^2 mol^{-1}); the absorption rises strongly at wavelengths below 235 nm toward a second peak in the vicinity of 197 nm ($\epsilon_{max} \approx 60$ m^2 mol^{-1}). At HN_3 concentrations of about 1 mmol dm^{-3} the radiation at wavelengths below 220 nm is almost fully absorbed in the solution, whereas radiation at longer wavelengths is less effective. This minimizes the absorption of a group of lines in the 240−280 nm wavelength range, which the zinc arc lamp emits in addition to the 213.9 nm line, albeit with much lower intensities.[15] Under these conditions the hydrazoic acid actinometer registers primarily the 213.9 nm line as well as two weaker lines at shorter wavelengths (202.6 and 206.2 nm, approximately). Solutions of hydrazoic acid were prepared by dissolving NaN_3 crystals and adding 70% perchloric acid until pH $\approx$ 2 was reached.

Reagents and Analyses. Analytical grade reagents and deionized water were used to prepare solutions with known concentrations for calibration, actinometry and photolysis experiments. Millimolar solutions of sulfite were prepared from crystalline $NaSO_3$, and millimolar solutions of hydrogen sulfite from aqueous $NaHSO_3$ (40%). Sulfur(IV) contents were checked iodometrically by the method of Custer and Natelson.[16] Standard anion chromatography was used for routine analysis of sulfate and SO_3^{2-}/HSO_3^-. In the latter case formaldehyde was added prior to the analysis to enhance the stability of sulfur(IV) by conversion to hydroxymethanesulfonate. Dithionate, $S_2O_6^{2-}$, and peroxodisulfate, $S_2O_8^{2-}$, were determined by reversed phase ion chromatography using tetrabutylammonium hydroxide as ion-pair-forming reagent. Na_2CO_3 was added as modifier, and a standard suppressor column reduced the background signal of the conductivity detector. Hydroxylamine was analyzed by cation chromatography. Hydrazoic acid was determined spectrophotometrically at 260 nm wavelength, ferrous ion was converted to the Fe(II)−phenanthroline complex and determined by spectrophotometry at 510 nm wavelength. A gas chromatograph equipped with a thermal conductivity detector was used to determine nitrogen. For this purpose the gases that evolved during irradiation were subsequently expanded from the photolysis cell into an evacuated auxiliary bulb of 100 cm^3 capacity, and samples were taken from there. The partitioning factor was measured with known amounts of nitrogen injected into the (unirradiated) solution before expansion. The recovery ratio was 0.44 ± 0.06, on average, which is slightly less than that expected from the volume ratio of the expansion bulb and the photolysis cell.

Results

Actinometry. Ferric oxalate actinometry, used with the mercury lamp, gave (2.60 ± 0.12) × 10^{17} photons s^{-1} entering the quartz cell. The value is based on the recommended quantum yield of 1.24 for ferrous ion formation.[12] Figure 2a shows for the photolysis of hydrazoic acid by the mercury lamp

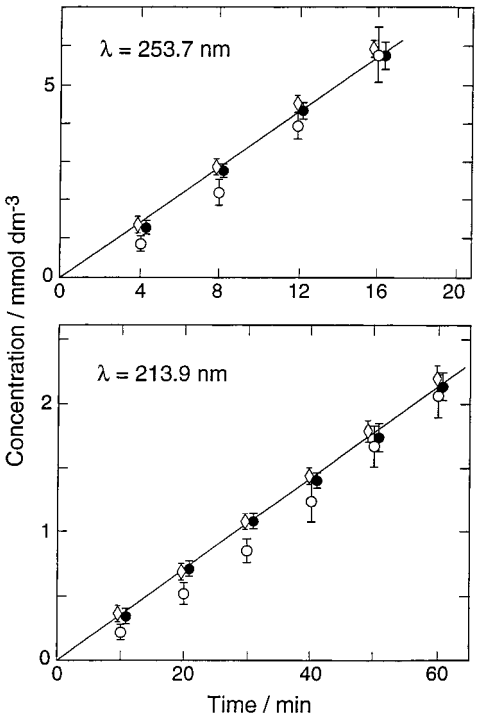

Figure 2. Hydrazoic acid actinometry, $[HN_3]_0 = 10$ mmol dm^{-3}: rise with time of nitrogen (open points) and NH_2OH (filled points) and loss of HN_3 (diamonds); (a, upper frame) mercury lamp; (b, lower frame) zinc lamp.

the production with time of hydroxylamine and nitrogen as well as the loss of HN_3. The linear rise in concentration of hydroxylamine matches that of the HN_3 loss. The rate of nitrogen production is initially somewhat lower but ultimately approaches that of hydroxylamine. Nitrogen, however, is determined with less precision than the other two quantities. The averages of the rates of HN_3 loss and NH_2OH production were used to calculate the effective radiation intensity. The amount of light absorbed in solution was calculated from the measured decadic absorption coefficient for HN_3 at 253.7 nm, $\epsilon = 4.43$ m^2 mol^{-1}. This resulted in (2.57 ± 0.10) × 10^{17} photons s^{-1}, in excellent agreement with the value obtained by ferric oxalate actinometry.

Figure 2b shows the temporal loss of HN_3 and the rise of NH_2OH and nitrogen in the photolysis of 10 mmol dm^{-3} hydrazoic acid solutions with the zinc lamp. The behavior is similar to that observed with the mercury lamp. The measured decadic absorption coefficient at 213.9 nm is 27.6 m^2 mol^{-1}. At the concentration used, 99.9% of 213.9 nm radiation is absorbed in the solution, but if lines at longer wavelength near 250 nm were present with similar intensity, they would markedly contribute to HN_3 photolysis. Accordingly, another set of measurements was made at lower concentration, $[HN_3]_0 = 1$ mmol dm^{-3}, which minimized the contribution of lines at longer wavelengths. The NH_2OH concentration and loss of HN_3 were again observed to rise linearly with time. The effective radiation intensity calculated from the measured rates of HN_3 loss for the two concentrations was (1.93 ± 0.06) × 10^{16} and (1.86 ± 0.10) × 10^{16} photons s^{-1}, respectively, whereas the NH_2OH production rates gave (1.87 ± 0.09) × 10^{16} and (1.67 ± 0.07) × 10^{16} photons s^{-1}. The values are quite consistent with each other, indicating that the influence of zinc emission lines at longer wavelengths is essentially negligible. An average value of (1.83 ± 0.13) × 10^{16} photons s^{-1} was used in subsequent experiments with S(IV) solutions.

Photodecomposition of Sulfite. Our previous study[6] of this process with a mercury lamp inferred a rather high primary

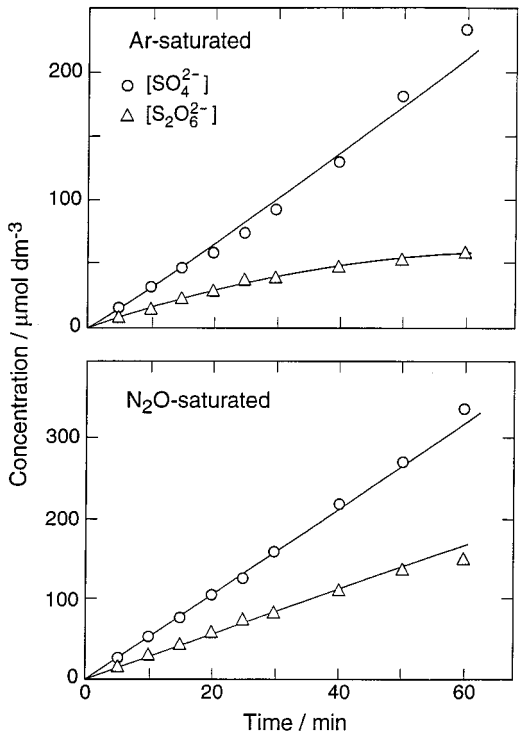

Figure 3. Rise of sulfate (open points) and dithionate (triangles) in the 253.7 nm photolysis of millimolar SO_3^{2-} solutions: (a, upper frame) argon-saturated; (b, lower frame) nitrous oxide-saturated. The solid lines in part a were calculated with the rate coefficients given in Table 1.

TABLE 1: Reactions Following the Photodecomposition of Sulfite Anion[a]

(1)	$SO_3^{2-} + h\nu \rightarrow SO_3^- + e_{aq}^-$	Φ_p
(2a)	$e_{aq}^- + N_2O\ (+H^+) \rightarrow OH + N_2$	$k_{2a} = 9.1 \times 10^9$ [b]
(2b)	$H + N_2O \rightarrow OH + N_2$	$k_{2b} = 2.1 \times 10^6$ [b]
(3)	$OH + SO_3^{2-} \rightarrow OH^- + SO_3^-$	$k_3 = 4.5 \times 10^9$ [b]
(4a)	$SO_3^- + SO_3^- \rightarrow S_2O_6^{2-}$	$2k_4 = 6.2 \times 10^8$ [c]
(4b)	$SO_3^- + SO_3^-\ (+H_2O) \rightarrow SO_4^{2-} + H^+ + HSO_3^-$	$k_{4a}/k_4 = 0.37$ [d]
(5a)	$e_{aq}^- + S_2O_6^{2-} \rightarrow SO_3^{2-} + SO_3^-$	$k_5 \approx 2 \times 10^5$ [d]
(5b)	$H + S_2O_6^{2-} \rightarrow HSO_3^- + SO_3^-$	$k_5 \approx 2 \times 10^5$ [d]
(6a)	$e_{aq}^- + H_2O \rightarrow H$	$k_{6a} = 19$ [b]
(6b)	$e_{aq}^- + H^+ \rightarrow H$	$k_{6b} = 2.3 \times 10^{10}$ [b]
(6c)	$H + OH^- \rightarrow e_{aq}^-$	$k_{6c} = 2.2 \times 10^7$ [b]
(7a)	$e_{aq}^- + e_{aq}^- \rightarrow H_2 + 2OH^-$	$2k_{7a} = 1.1 \times 10^{10}$ [b]
(7b)	$e_{aq}^- + H\ (+H_2O) \rightarrow H_2 + OH^-$	$k_{7b} = 2.5 \times 10^{10}$ [b]
(7c)	$H + H \rightarrow H_2$	$2k_{7c} = 1.6 \times 10^9$ [b]
(8a)	$e_{aq}^- + SO_3^- \rightarrow SO_3^{2-}$	*e*
(8b)	$H + SO_3^- \rightarrow HSO_3^-$	*e*

[a] Unit of rate coefficients: $dm^3\ mol^{-1}\ s^{-1}$. [b] Reference 18. [c] Reference 20. [d] Present data. [e] Neglected; see text.

quantum yield of 0.85 with $[SO_3^{2-}] \approx 0.5$ mmol dm^{-3}. However, the quantum yield decreased when the sulfite concentration was increased,[17] indicating a variable absorption possibly due to light at 185 nm wavelength, which is emitted from the mercury lamp together with the 253.7 nm line. At that time no effort was made to eliminate 185 nm radiation. This omission was corrected in the present study. Figure 3 shows the evolution of sulfate and dithionate in the photolysis of millimolar SO_3^{2-} solutions saturated with either argon or nitrous oxide. Table 1 gives a mechanism to explain the formation of these products. They result mainly from the recombination and disproportionation of SO_3^- radicals. N_2O acts as a scavenger of hydrated electrons and converts them to OH radicals. Their reaction with sulfite produces another sulfite radical, so that the yield is doubled. Product evolution in solutions saturated with N_2O is essentially linear with time. In argon-saturated solutions sulfate rises more strongly at later times than initially, at the expense of dithionate. This behavior is attributed to reactions of hydrated electrons with dithionate, reaction 5a, assisted somewhat by reaction with hydrogen atoms, reaction 5b. At pH 9, the equilibrium between e_{aq}^- and H is perturbed, because reaction 6a is fairly slow, leading to an excess concentration of e_{aq}^- compared to pK = 9.6, in steady state with hydrogen atoms. The solid lines shown in Figure 3a were calculated on the basis of the mechanism in Table 1 with the rate coefficients given there.

TABLE 2: Photodecomposition of Sulfite in Aqueous Solution: Average Conversion Rates, Quantum Yields, and Product Ratios

$[SO_3^{2-}]$ (mmol dm^{-3})	$\Delta[SO_3^{2-}]/\Delta t$ (nmol $dm^{-3}\ s^{-1}$)	Φ_c	$\Phi(SO_3^-)$	$[S_2O_6^{2-}]/[SO_4^{2-}]$
	Argon-Saturated			
0.5	1.0 ± 0.1	0.23 ± 0.01	0.34 ± 0.02	0.49 ± 0.02
0.75	1.7 ± 0.1	0.25 ± 0.01	0.38 ± 0.02	0.46 ± 0.04
1.0	2.5 ± 0.1	0.28 ± 0.01	0.42 ± 0.02	0.48 ± 0.05
2.5	5.8 ± 0.2	0.27 ± 0.02	0.40 ± 0.02	0.47 ± 0.01
5.0	9.9 ± 0.7	0.25 ± 0.01	0.37 ± 0.03	0.48 ± 0.06
average		0.25 ± 0.02	0.39 ± 0.04	0.48 ± 0.04
	Nitrous Oxide-Saturated			
0.5	2.1 ± 0.2	0.49 ± 0.03	0.71 ± 0.05	0.62 ± 0.02
0.75	3.4 ±0.1	0.52 ± 0.02	0.76 ± 0.03	0.60 ± 0.03
1.0	4.5 ± 0.1	0.52 ± 0.02	0.77 ± 0.02	0.59 ± 0.02
2.5	10.5 ± 0.4	0.51 ± 0.02	0.74 ± 0.03	0.60 ± 0.04
5.0	19.7 ± 1.1	0.50 ± 0.03	0.72 ± 0.05	0.62 ± 0.02
average		0.51 ± 0.03	0.75 ± 0.04	0.61 ± 0.03

The calculation of quantum yields is based on the formula

$$\Phi_c = \frac{\Delta[SO_3^{2-}]/\Delta t}{I_0\{1 - 10^{-\epsilon c d}\}/V_k N_A} \qquad \text{(E1)}$$

where $\Delta[SO_3^{2-}]/\Delta t$ is the rate of sulfite consumption, $I_0 = 2.6 \times 10^{17}$ photons s^{-1}, $\epsilon = 1.76\ m^2\ mol^{-1}$, $c = 10^3\ [SO_3^{2-}]$ with the concentration in mol dm^3, $d = 1.15 \times 10^{-2}$ m is the optical path length, V_k is the volume of the photolysis cell, and $N_A = 6.02 \times 10^{23}$ is Avogadro's number. The quantum yield for SO_3^- radicals is related to that of sulfite consumption by

$$\Phi(SO_3^-) = \Phi_c \frac{2([SO_4^{2-}] + [S_2O_6^{2-}])}{([SO_4^{2-}] + 2[S_2O_6^{2-}])} \qquad \text{(E2)}$$

provided secondary losses of products can be neglected. Table 2 lists values of both quantum yields for different sulfite concentrations. Because of the variation in the production rates, and to avoid an excessive consumption of sulfite, only the first five data points at times up to 25 min were used in calculating averages. The values are markedly lower than that reported previously, but they are independent of concentration. This shows that the problem mentioned above has been removed. The average value in argon-saturated solution is $\Phi(SO_3^-) = 0.39 \pm 0.04$. It agrees well with half of that obtained in nitrous oxide-saturated solution $(0.75 \pm 0.04)/2 = 0.38 \pm 0.02$, which is expected if the hydrated electrons are largely converted to OH radicals and these react further with sulfite. In addition, this result indicates that the direct recombination of SO_3^- with hydrated electrons or hydrogen atoms can be neglected. Accordingly, $\Phi(SO_3^-)$ in argon-saturated solution is equivalent to the primary quantum yield Φ_p. Ratios of dithionate to sulfate, which are given in Table 2, are independent of sulfite concentration, but they are markedly higher in the presence of N_2O compared to argon-saturated solutions. This behavior is again attributed to the influence of reaction 5a, which is suppressed by the addition of N_2O. In this case the average ratio is $[S_2O_6^{2-}]/[SO_4^{2-}] = 0.61 \pm 0.03$. This value gives the branching ratio of reaction 4, $k_{4a}/k_4 = 0.37 \pm 0.02$.

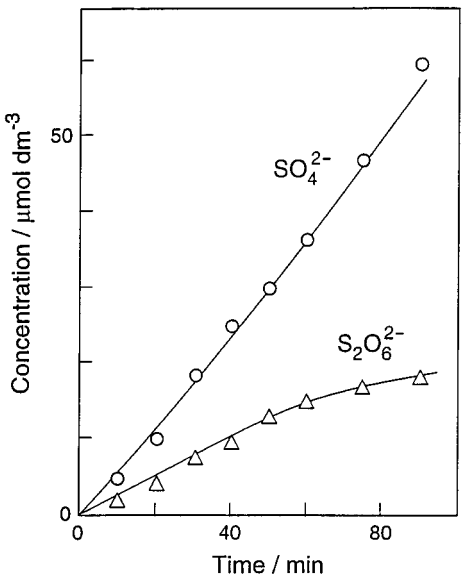

Figure 4. Evolution of products in the photodecomposition of HSO_3^- in argon-saturated aqueous solution; $[HSO_3^-]_0 = 1$ mmol dm^{-3}. The solid lines were calculated with the rate coefficients given in Table 1.

Photodecomposition of Hydrogen Sulfite. Sulfate and dithionate were observed as products when argon-saturated HSO_3^- solutions were irradiated with light from the zinc lamp. The dithionate/sulfate ratio was about the same as that observed in the photolysis of sulfite. This is taken as evidence that HSO_3^- undergoes photodecomposition to generate SO_3^- radicals. Figure 4 shows the rise of product concentrations with time. The reaction mechanism for the photodecomposition of HSO_3^- is taken to consist of the primary step

$$HSO_3^- + h\nu \rightarrow SO_3^- + H \qquad (9)$$

followed by reactions 4, 5b, and 7c. In the pH range 4−5 the concentration of hydrated electrons is 4−5 orders of magnitude lower than at pH 9, so that their reactions can be neglected to a first approximation. The primary process 9, as pointed out by a reviewer, may involve the reaction sequence

$$HSO_3^- + h\nu \rightarrow HSO_3 + e_{aq}^- \qquad (9a)$$

$$HSO_3 \rightarrow H^+ + SO_3^- \qquad (10)$$

$$e_{aq}^- + H^+ \rightarrow H \qquad (6c)$$

which cannot be distinguished from the direct formation of a hydrogen atom in reaction 9. The solid lines in Figure 4 were calculated on the basis of this mechanism ($\Phi_p = 0.19$) and with the rate constants shown in Table 1. It was not possible, however, to fit the data with $k_{4a}/k_4 = 0.37$. Instead, it was necessary to reduce the value to about 0.30.

Reaction 4b is a source of hydrogen ions. Whereas in the photolysis of sulfite at pH ≈ 9 reaction 4b does not fully compensate the consumption of hydrogen ions by reactions 6b and 7 (or 2a and 3) so that the pH of the system rises, the photolysis of HSO_3^- does not involve reaction 6. The solution accordingly acidifies. The initial pH derived after preparing the solution was slightly below pH 5 for $[HSO_3^-] = 1$ mmol dm^{-3}. Figure 5 shows that the rate of hydrogen ion production estimated from the change in pH agrees well with that of sulfate production, which is expected on the basis of the suggested mechanism.

Table 3 presents quantum yields for the photodecomposition of HSO_3^- for a range of concentrations in both argon- and nitrous oxide-saturated solutions. Equations E1 and E2 were again used to derive the quantum yields. The decadic absorption coefficient was $\epsilon = 8.9$ m^2 mol^{-1}, measured at 213.9 nm wavelength. The consumption of HSO_3^- was negligible in both cases. Samples were taken every 10 min for irradiations lasting 1 h, and the results were averaged. There is no great dependence on the concentration of HSO_3^-. The overall average is 0.19 ± 0.03 for the primary quantum yield of sulfite radicals from HSO_3^- in argon-saturated solutions. At an initial pH ≈ 5 the true quantum yield may be somewhat lower, because the strong absorption of SO_3^{2-} at 213.9 nm wavelength (see Figure 1) contributes about 16% to the total absorption of sulfur(IV). With increasing time of irradiation the pH decreases, so that the concentration of SO_3^{2-} and its contribution to total absorption decrease as well. However, the experimental scatter at short irradiation times prevented this effect from showing up in the individual quantum yields determined at different irradiation times.

In contrast to the results for SO_3^{2-} the presence of N_2O did not double the quantum yield, although it did raise the values somewhat. While the rate constant for the reaction of H atoms with N_2O is over 3 orders of magnitude smaller than that for hydrated electrons (see Table 1), it is still fully competitive with

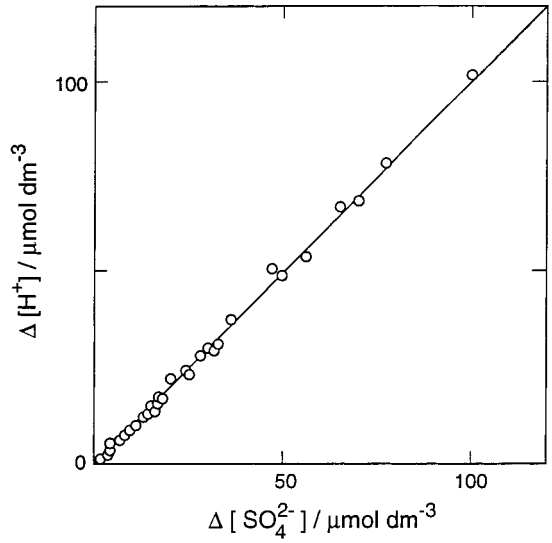

Figure 5. Photodecomposition of HSO_3^- in argon-saturated aqueous solution: equivalence of hydrogen ion and sulfate production rates. The solid line indicates a 1:1 ratio.

TABLE 3: Photodecomposition of HSO_3^- in Aqueous Solution: Average Conversion Rates, Quantum Yields, and Product Ratios

$[HSO_3^-]$ (mmol dm^{-3})	$\Delta[HSO_3^-]/\Delta t$ (nmol dm^{-3} s^{-1})	Φ_c	$\Phi(SO_3^-)$	$[S_2O_6^{2-}]/[SO_4^{2-}]$
		Argon-Saturated		
0.5	8.5 ± 0.9	0.11 ± 0.02	0.17 ± 0.02 (0.16)[a]	0.41 ± 0.02
0.75	12.7 ± 1.6	0.12 ± 0.02	0.19 ± 0.02 (0.18)	0.39 ± 0.02
1.0	16.5 ± 2.0	0.13 ± 0.02	0.20 ± 0.03 (0.19)	0.39 ± 0.02
2.5	37.0 ± 3.5	0.12 ± 0.02	0.19 ± 0.03 (0.21)	0.42 ± 0.02
5.0	55.0 ± 4.9	0.13 ± 0.01	0.20 ± 0.02 (0.23)	0.41 ± 0.02
average		0.12 ± 0.03	0.19 ± 0.03	0.40 ± 0.03
		Nitrous Oxide-Saturated		
0.5	10.8 ± 1.3	0.14 ± 0.02	0.22 ± 0.03	0.45 ± 0.05
0.75	16.7 ± 1.7	0.16 ± 0.02	0.25 ± 0.03	0.43 ± 0.03
1.0	21.3 ± 1.4	0.16 ± 0.01	0.25 ± 0.02	0.40 ± 0.01
2.5	44.6 ± 4.9	0.16 ± 0.02	0.24 ± 0.03	0.43 ± 0.01
5.0	68.0 ± 8.7	0.16 ± 0.02	0.24 ± 0.03	0.42 ± 0.01
average		0.16 ± 0.02	0.25 ± 0.04	0.43 ± 0.04

[a] Values in parentheses were calculated with the assumption that SO_3^- radicals are partly produced by H atoms reacting with HSO_3^-; see text.

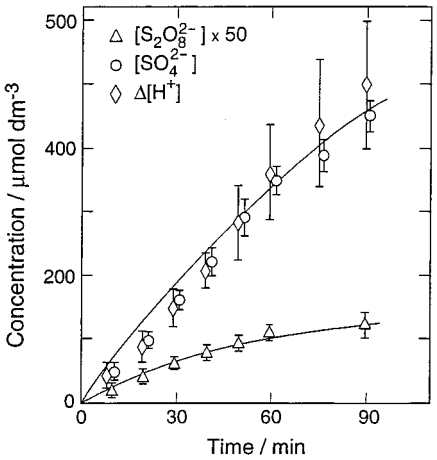

Figure 6. Evolution of products in the photooxidation of HSO_3^- in aerated aqueous solution; $[HSO_3^-]_0 = 1$ mmol dm^{-3}. The solid lines were calculated with a simple steady state approximation (see text).

H atom recombination, reaction 7c, so that all the H atoms should be scavenged. If the SO_3^- quantum yield in the presence of N_2O were twice the primary quantum yield, its value would be $\Phi_p \approx 0.12$. The higher SO_3^- quantum yield in argon-saturated solution (0.19 versus 0.12) would then require another source of SO_3^- at the expense of hydrogen atoms. This suggests the occurrence of the reaction

$$H + HSO_3^- \rightarrow H_2 + SO_3^- \quad (11)$$

which would cause the SO_3^- quantum yield to depend on HSO_3^- concentration, in contrast to the near independence of the data in Table 3. Sample calculations showed, however, that a rate coefficient $k_{11} \approx 2 \times 10^4$ dm^3 mol^{-1} s^{-1} would suffice to generate the additional amount of sulfite radicals needed. SO_3^- quantum yields calculated with this assumption for argon-saturated solutions are included in Table 3 (in parentheses). The values fall mostly within the range of the experimental uncertainties, so that reaction 11 is still compatible with the experimental data. The alternative explanation that less than one hydrogen atom is formed for each SO_3^- radical would be in conflict with the assumed primary process. Steady state calculations based on reaction 9 with $\Phi_p = 0.12$, followed by reactions 11, 4, 5b, and 7c, also reproduced the solid lines in Figure 4, but it was again necessary to set $k_{4a}/k_4 = 0.30$ in order to obtain a reasonable fit to the experimental data.

Table 3 also gives averages for the ratio of dithionate to sulfate. The values are slightly higher in the presence of N_2O compared with argon-saturated solutions. Yet even in this cases they are distinctly smaller than those obtained in the photodecomposition of sulfite, although in both sets of experiments the rise of products was observed to be linear with time. The observation that the ratios are essentially independent of HSO_3^- concentration indicates that the conceivable reaction

$$SO_3^- + HSO_3^- \rightarrow S_2O_6^{2-} + H \quad (12)$$

does not need to be taken into account.

Photooxidation of Hydrogen Sulfite. The products observed to result from the photolysis of HSO_3^- in oxygen-saturated solutions were sulfate, hydrogen ion, and peroxodisulfate, the latter in small amounts. Compared to sulfite in alkaline medium, hydrogen sulfite in acidic solution is quite stable against autoxidation in the dark. Only minor corrections for sulfate formation in the dark were required. Figure 6 shows the rise of product concentrations with time of irradiation. The rise in hydrogen ion concentration estimated from pH measurements follows that of sulfate despite the greater scatter. The following mechanism was used for a quantitative interpretation of the data:

$$HSO_3^- + h\nu \rightarrow SO_3^- + H \quad (9)$$

$$k_9 = 2.9 \times 10^{-5}\ s^{-1}$$

$$SO_3^- + O_2 \rightarrow SO_5^- \quad (13)$$

$$k_{13} = 2.5 \times 10^9$$

$$H + O_2 \rightarrow HO_2 \quad (14)$$

$$k_{14} = 7.5 \times 10^9$$

$$HO_2 \rightarrow H^+ + O_2^- \quad (15)$$

$$pK_{15} = 4.8$$

$$SO_5^- + HSO_3^- \rightarrow HSO_5^- + SO_3^- \quad (16a)$$

$$k_{16a} = 8.5 \times 10^3$$

$$SO_5^- + HSO_3^- \rightarrow SO_4^{2-} + H^+ + SO_4^- \quad (16b)$$

$$k_{16b} = 0.04k_{14}$$

$$SO_4^- + HSO_3^- \rightarrow SO_4^{2-} + H^+ + SO_3^- \quad (17)$$

$$k_{17} = 6.8 \times 10^8$$

$$SO_5^- + SO_5^- \rightarrow S_2O_8^{2-} + O_2 \quad (18a)$$

$$k_{18a} = 9.3 \times 10^7$$

$$SO_5^- + SO_5^- \rightarrow 2SO_4^- + O_2 \quad (18b)$$

$$k_{18b} = 7k_{16a}$$

$$SO_5^- + HO_2 \rightarrow HSO_5^- + O_2 \quad (19a)$$

$$k_{19a} = 1.7 \times 10^9$$

$$SO_5^- + O_2^- (+H^+) \rightarrow HSO_5^- + O_2 \quad (19b)$$

$$k_{19b} = 2.7 \times 10^8$$

$$HO_2 + HO_2 \rightarrow H_2O_2 + O_2 \quad (20a)$$

$$k_{20a} = 8.3 \times 10^5$$

$$HO_2 + O_2^- (+H^+) \rightarrow H_2O_2 + O_2 \quad (20b)$$

$$k_{20b} = 9.7 \times 10^8$$

$$HSO_5^- + HSO_3^- \rightarrow 2H^+ + 2SO_4^{2-} \quad (21)$$

$$k_{21} \approx 1 \times 10^3$$

$$H_2O_2 + HSO_3^- \rightarrow H^+ + SO_4^{2-} + H_2O \quad (22)$$

$$k_{22} \approx 1 \times 10^3$$

This mechanism is equivalent to one used previously in a discussion of the photooxidation of sulfite in the alkaline pH region.[6] The rate coefficients are largely known, although not all of them have so far been published in the open literature. The values quoted were taken from refs 18−20. The rate coefficients for reactions 21 and 22 are pH dependent, and the values listed refer to pH ≈ 4. The value for k_{18a}, which serves partly as a scaling factor in the data evaluation, is an average of four values: 0.5, 1.0, 0.93, and 1.3 (unit: 10^8 dm^3 mol^{-1} s^{-1}) taken from refs 21−24, respectively. Reactions 16a and 16b are the chain-propagating steps, but for the experimental conditions used, the chain is not well developed so that termination reactions are important. This opens the possibility

to check on values for some of the rate coefficients, especially k_{16} and k_{19a}. If peroxodisulfate arises exclusively from reaction 18a and radicals are assumed to be in a steady state, the kinetic treatment of the above mechanism leads to the following equations for the production of peroxodisulfate and the consumption of sulfite, respectively.

$$d[S_2O_8^{2-}]/dt = (k_9/A)X \quad \text{(E3)}$$

$$dX/dt = 2k_9\{1 + ((k_{18b}/k_{18a}) - 3/2)/A\}X + 2k_{16}(k_9/k_{18a}A)^{1/2}X^{3/2} \quad \text{(E4)}$$

where $X = [HSO_3^-]$, $k_9 = \Phi_p I_0 \epsilon d(\ln 10)/V_k N_A = 2.9 \times 10^{-5}$ s^{-1} (for $\Phi_p = 0.19$).

$$-d[HSO_3^-]/dt = -dX/dt = d[SO_4^{2-}]/dt + 2d[S_2O_8^{2-}]/dt$$

$$A = 2 + (k_{19eff}/k_{18a})(k_{18a}/k_{20eff})^{1/2}$$

k_{19eff} and k_{20eff} are compound rate coefficients for reactions of HO_2 defined by

$$k_{19eff} = k_{19a} + k_{19b}(K_{15}/[H^+]) \approx k_{19a}$$

$$k_{20eff} = k_{20a} + {}^1/_2 k_{20b}(K_{15}/[H^+])$$

This is to simplify the treatment of HO_2 reactions, which occur partly via the O_2^- radical due to the equilibrium 15 and thus are pH dependent. In the first case $k_{19b} \ll k_{19a}$, and at values below pH 5 reaction 19b is essentially negligible compared with reaction 19a. In the second case $k_{20b} \gg k_{20a}$, so that the full expression must be used. Moreover, as $[H^+]$ varies with time, k_{20eff} decreases from about 4×10^8 at the beginning to 2×10^7 toward the end of irradiation (unit: $dm^3\ mol^{-1}\ s^{-1}$). In the evaluation of eq E3, the variation of k_{20eff} as well as that of $[HSO_3^-]$ was taken into account. From the data shown in Figure 6 one obtains for the ratio the average value

$$k_{19a}/k_{18a} = \{k_9X/(d[S_2O_8^{2-}]/dt) - 2\}/(k_{18a}/k_{20eff})^{1/2} = 23.5 \pm 8.4$$

which with $k_{18a} = 9.3 \times 10^7\ dm^3\ mol^{-1}\ s^{-1}$ leads to $k_{19a} = (2.2 \pm 0.8) \times 10^9\ dm^3\ mol^{-1}\ s^{-1}$.

Equation E4 has the solution

$$(X_0/X)^{1/2} = -(b/a)X_0^{1/2} + (1 + (b/a)X_0^{1/2})\exp({}^1/_2 at) \quad \text{(E5)}$$

where $a = 2k_9(1 + ((k_{18b}/k_{18a}) - 3/2)/A\}$ and $b = 2k_{16}(k_9/k_{18a}A)^{1/2}$ are the factors appearing on the right-hand side of eq 4. The ratio $k_{18b}/k_{18a} \approx 7$ has recently been determined by Yermakov et al.;[9] the parameter A was determined in conjunction with k_{19a}/k_{18a} and was found to be $A = 37.8 \pm 5.1$, on average; with these values the parameter a is calculated to be $a = 2.33k_9$. Figure 7 shows a plot of $(X_0/X)^{1/2}$ versus $\exp({}^1/_2 at)$. The straight line shown results from a linear regression analysis of the data leading to $y = -(0.91 \pm 0.10) + (1.89 \pm 0.10)\exp({}^1/_2 at)$. Slope and intercept with the ordinate give $(b/a)X_0^{1/2} = 0.90 \pm 0.10$, from which one obtains $k_{16} = (1.1 \pm 0.3) \times 10^4\ dm^3\ mol^{-1}\ s^{-1}$. The error margin for k_{16} includes the uncertainties inherent in the values of A and a, which are larger than the scatter of the data points. A similar result would have been obtained if the data for $\Delta[H^+]$ shown in Figure 6 had been included in the evaluation, despite their larger scatter compared to $\Delta[SO_4^{2-}]$. The curves in Figure 6 were derived by computer simulation based on the above rate coefficients. The curves are in reasonable agreement with the experimental data.

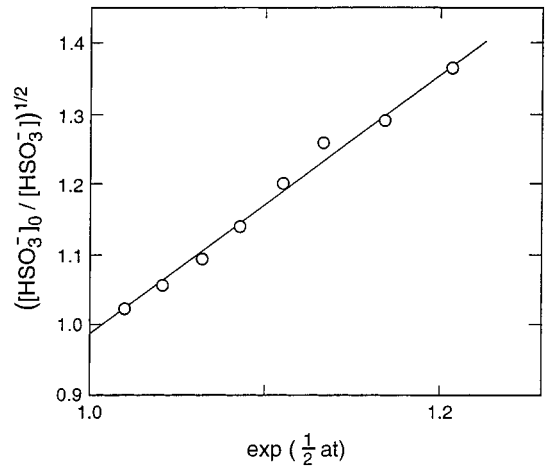

Figure 7. Plot of $([HSO_3^-]_0/[HSO_3^-])^{1/2}$ versus $\exp({}^1/_2 at)$. The linear regression line is represented by $y = -(0.91 \pm 0.11) + (1.89 \pm 0.10)x$.

Because of the uncertainties inherent in the primary quantum yield for $[HSO_3^-]$ photodissociation, the procedure was repeated with the assumption that $\Phi_p = 0.12$. This gave $k_{19a} = (1.4 \pm 0.6) \times 10^9$ and $k_{16} = (1.3 \pm 0.3) \times 10^4\ dm^3\ mol^{-1}\ s^{-1}$. These values agree in magnitude with those derived above. Both sets of values may be combined to obtain a range of values $k_{19a} = (1.8 \pm 1.0) \times 10^9$ and $k_{16} = (1.2 \pm 0.4) \times 10^4\ dm^3\ mol^{-1}\ s^{-1}$.

Discussion

The present study confirms that sulfite radicals and hydrated electrons are the principal products in the photodecomposition of sulfite. This is made evident especially by the results with N_2O as a scavenger for hydrated electrons. The photodecomposition of hydrogen sulfite likewise produces sulfite radicals. In this case the effect of N_2O is smaller. The quantum yields determined in argon-saturated solutions for the photolysis of SO_3^{2-} at 253.7 nm and for HSO_3^- at 213.9 nm wavelength are 0.39 ± 0.04 and 0.19 ± 0.03, respectively. Both are essentially independent of concentration in the range used. In the first case the quantum yield is smaller than that reported previously, but those data were probably influenced by the presence of radiation at wavelengths shorter than 253.7 nm, which is now eliminated. However, even the lower value 0.39 indicates a significant quantum yield. The primary SO_3^- quantum yield in the photolysis of HSO_3^- is uncertain. If the yield measured in the presence of N_2O represents twice the primary quantum yield as in the case of SO_3^{2-}, the primary quantum yield would be $\Phi_p \approx 0.12$. In this case, hydrogen atoms would have to react with HSO_3^- to produce the additional SO_3^- radicals observed in argon-saturated solutions. Our results also confirm that the products resulting from the self-reaction of sulfite radicals are dithionate and sulfate. The ratio given previously[6] was 0.5. The present results indicate that the ratio varies somewhat with experimental conditions. The values obtained in the presence of N_2O in order to eliminate possible perturbing reactions of hydrogen atoms and hydrated electrons are 0.61 ± 0.03 at pH 9 (SO_3^{2-} photolysis) and 0.43 ± 0.04 at pH 5 (HSO_3^- photolysis). Since the rate coefficient for reaction 4 shows no pH dependence,[20] the branching ratio k_{4a}/k_4 likewise is not expected to depend on pH. The mechanism in Table 1 assumes that reaction 4 is the sole source of dithionate and sulfate. Additional sources of dithionate in alkaline or sulfate in acidic solution are not obvious. The reaction $SO_3^- + HSO_3^- \rightarrow H +$

$S_2O_6^{2-}$ would increase rather than reduce the concentration of dithionate, and the independence of the $[S_2O_6^{2-}]/[SO_4^{2-}]$ ratio with HSO_3^- concentration also argues against this reaction. Accordingly, it appears that k_{4a}/k_4 has a value in the range 0.30−0.37, but we are unable to determine it more precisely.

Application of the zinc arc lamp allowed a study of the photooxidation of HSO_3^- in aerated solution. Although this process is a chain reaction, the chain length L is rather short. This parameter is given by the second term on the right-hand side of eq 4, divided by $2k_0[HSO_3^-]$ (two sulfate molecules are produced in each step), plus a term dealing with propagation by reaction 18b followed by reaction 17:

$$L = k_{16}([HSO_3^-]/k_9k_{18a}A)^{1/2} + 2k_{18b}/k_{18a}A \qquad \text{(E6)}$$

From the numerical data derived in the Results section one calculates a chain length of $L \approx 1.5$, with the second term in eq 6 contributing about 25% to the total. The rate of sulfate production is comparable to that associated with chain termination by reaction 19. The short chain length in the photooxidation of HSO_3^- in acidic solution contrasts with that of SO_3^{2-} in the akaline pH region, for which a chain length of about 300 has been found under similar experimental conditions.[6] The major reason for the difference lies in the smaller value for the rate coefficient of the propagation reaction 16 when HSO_3^- is involved ($k_{16} \approx 1 \times 10^4$ dm^3 mol^{-1} s^{-1}) compared to SO_3^{2-} ($k_{16}' \approx 5 \times 10^5$ dm^3 mol^{-1} s^{-1}). In addition it must be noted that the rate constant for the principal termination reaction in acidic solution, which involves SO_5^- and HO_2, is greater compared with that in alkaline solution, which involves SO_5^- and O_2^- (reactions 19a and 19b, respectively). The expression for the chain length contains the rate coefficients for chain termination underneath a square root and the rate constants for the propagation reactions as a proportionality factor. Termination by the self-reaction of two SO_5^- radicals is not very pronounced as long as HO_2 or O_2^- radicals are present. Buxton et al.[8] have observed much greater chain lengths in the steady state γ-radiolysis of hydrogen sulfite and sulfite, about 75 and 6100, respectively. In their experiments the formation of HO_2 and O_2^- radicals was suppressed, and the termination reaction was mainly the self-reaction of SO_5^- radicals, reaction 18a, which is comparatively slow.

The evaluation of data obtained from the photooxidation experiments relies on the assignment of $S_2O_8^{2-}$ as sole product from the self-reaction of SO_5^- radicals, reaction 18a. This is the first time that peroxodisulfate was observed as a product in the photooxidation of S(IV). The rate of $S_2O_8^{2-}$ formation was used to derive the rate coefficient k_{19a}, which was found to lie in the range $(1.8 \pm 1.0) \times 10^9$ dm^3 mol^{-1} s^{-1}. The wide error margin is partly due to the pH change and its influence on the recombination of HO_2/O_2^- radicals during the photooxidation process but more importantly due to uncertainties about the primary quantum yield for the HSO_3^- photodecomposition. Nevertheless, the value is in good agreement with one recently derived from pulse radiolysis experiments,[20,25] $k_{19a} = (1.7 \pm 0.1) \times 10^9$ dm^3 mol^{-1} s^{-1}. The present value also agrees approximately with $k_{19a} = 4.3 \times 10^9$ dm^3 mol^{-1} s^{-1}, which was found necessary to reproduce, by computer simulation, experimental data for the oxidation of HSO_3^- in the presence of iron as catalyst, with and without the addition of benzene as scavenger for sulfate radicals.[11] Thus, a reasonable degree of consistency has been reached for this rate coefficient from three different experimental systems.

The second rate coefficient that was derived from the present data is k_{16}, which was found to fall in the range $k_{16} = (1.2 \pm 0.4) \times 10^4$ dm^3 mol^{-1} s^{-1}. The steady state γ-radiolysis experiments[8] gave $k_{16} = 1.2 \times 10^4$ dm^3 mol^{-1} s^{-1} when $2k_{18a} = 1.8 \times 10^8$ dm^3 mol^{-1} s^{-1} was used in evaluating the data, or 8.5×10^3 dm^3 mol^{-1} s^{-1} when $2k_{18a} = 1.0 \times 10^8$ dm^3 mol^{-1} s^{-1} was employed.[20,21] Within the margin of uncertainty the present result is consistent with both. Again it appears that a consensus has been reached on an important rate constant in the sulfur(IV) chain oxidation system.

Finally it should be mentioned that attempts in the present study to use either ethanol or 2-propanol as scavengers for SO_4^- radicals in the photooxidation of HSO_3^- failed, because both alcohols undergo photolysis at the short wavelengths emitted by the zinc lamp. The photolysis products were the same as those resulting from the scavenging reaction. Thus it was not possible to check on the presence of sulfate radicals in the system. The production of SO_4^- by reaction 16b appears to be minor according to recent experimental data[11,26] for the iron-catalyzed oxidation of HSO_3^-, but it would have been of interest to confirm the extent of SO_4^- production in reaction 18b, which contributes to a continuation of the chain.

Acknowledgment. The present work, a contribution to EUROTRAC Subproject HALIPP, was performed within the Sonderforschungsbereich 233 (Dynamics and Chemistry of Hydrometeors), which is supported by the Deutsche Forschungsgemeinschaft.

References and Notes

(1) Brandt, C.; van Eldik, R. *Chem. Rev.* **1995**, *95*, 119−190.
(2) Bäckström, H. L. J. *Z. Phys. Chem.* **1934**, *25B*, 122−138.
(3) Hayon, E.; Treinin, A.; Wilf, J. *J. Am. Chem. Soc.* **1971**, *94*, 47−57.
(4) Bäckström, H. L. J. *J. Am. Chem. Soc.* **1927**, *49*, 1460−1472.
(5) Haber, F.; Wansbrough-Jones, O. H. *Z. Phys. Chem.* **1932**, *18B*, 103−123.
(6) Deister, U.; Warneck, P. *J. Phys. Chem.* **1990**, *94*, 2191−2198.
(7) Huie, R. E.; Neta, P. *Atmos. Environ.* **1987**, *21*, 1743−1747.
(8) Buxton, G. V.; McGowan, S.; Salmon, G. A. In *Proceedings of EUROTRAC Symp. '92*; Borrell, P. M., Borrell, P., Cvitas, T., Seiler, W., Eds.; SPB Academic Publ.: The Hague, The Netherlands, 1993; pp 599−604.
(9) Yermakov, A. N.; Zhitomirsky, B. M.; Poskrebyshev, G. A.; Sozurakov, D. M. *J. Phys. Chem.* **1993**, *97*, 10712−10714.
(10) Connick, R. E.; Zhang, Y.-X.; Lee, S.; Adamic, R.; Chieng, P. *Inorg. Chem.* **1995**, *34*, 4543−4553.
(11) Ziajka, J.; Beer, F.; Warneck, P. *Atmos. Environ.* **1994**, *26A*, 2549−2552.
(12) Hatchard, C. G.; Parker, C. A. *Proc. R. Soc. London A* **1956**, *235*, 518−536.
(13) Shapira, D.; Treinin, A. *J. Phys. Chem.* **1973**, *77*, 1195−1198.
(14) Deister, U.; Neeb, R.; Helas, G.; Warneck, P. *J. Phys. Chem.* **1986**, *90*, 3213−3217.
(15) Weast, R. C., Ed. *CRC Handbook of Chemistry and Physics*, 64th ed.; CRC Press: Boca Raton, FL, 1984.
(16) Custer, J. J.; Natelson, S. *Anal. Chem.* **1949**, *21*, 1005−1009.
(17) Deister, U. Ph.D. Thesis, University Mainz, 1988.
(18) Buxton, G. V.; Greenstock, C. L.; Helman, W. P.; Ross, A. B. *J. Phys. Chem Ref. Data* **1988**, *17*, 513−886.
(19) Bielski, B. H. J.; Cabelli, D. E.; Arudi, R. L.; Ross, A. B. *J. Phys. Chem. Ref. Data* **1985**, *14*, 1041−1100.
(20) Warneck, P., Ed. *Transport and Chemical Transformation of Pollutants in the Troposphere, Part 6: Heterogeneous and Liquid Phase Reactions*; Springer: Berlin, in press.
(21) Buxton, G. V.; McGowan, S.; Salmon, G. A.; Williams, J. E.; Wood, N. D. *Atmos. Environ.* **1996**, *30*, 2483.
(22) Huie, R. E.; Clifton, C. L.; Altstein, N. *Radiat. Phys. Chem.* **1989**, *33*, 361−370.
(23) Waygood, S. J. In *Laboratory Studies on Atmospheric Chemistry*; Cox, R. A., Ed.; Commission of the European Communities Air Pollution Research Report 42; Guyot: Brussels, 1992; pp 23−26.
(24) Herrmann, H.; Reese, A.; Zellner, R. In *Proceedings of EUROTRAC Symp. '92*; Borrell, P. M., Borrell, P., Cvitas, T., Seiler, W., Eds.; SPB Academic Publ.: The Hague, The Netherlands, 1994; pp 1017−1020.
(25) Buxton, G. V.; Malone, T. N.; Salmon, G. A. Leeds University, to be published.
(26) Ziajka, J.; Warneck, P. *Ber. Bunsen-Ges. Phys. Chem.* **1995**, *99*, 59−65.

JP953236B